Received: 20 June 2020 | Revised: 3 December 2020 | Accepted: 3 December 2020

DOI: 10.1002/pat.5195

RESEARCH ARTICLE

polymers for advanced technologies WILEY

Effect of ionic liquid octyltriphenylphosphonium-chelated orthoborates on flame retardance of epoxy

Yongliang Guo | Xiaodong Chen | Jinfeng Cui | Junhong Guo | Haojun Zhang | Baoping Yang

Department of Chemical Engineering, College of Petrochemical Technology, Lanzhou University of Technology, Lanzhou, China

Correspondence
Baoping Yang, Department of Chemical Engineering, College of Petrochemical Technology, Lanzhou University of Technology, Lanzhou 730050, China.
Email: yangbaoping2004@163.com

Abstract

Flame retardants (FRs) improve the intrinsic flammability of epoxy resins (EPs). However, the fundamental properties of EPs are inevitably compromised with the improvement of flame retardancy due to addition of FRs. Here, an ionic liquid (IL) octyltriphenylphosphonium-chelated orthoborate ([OTP][BScB]) has been synthesized and used as a flame-retarding additive for EP (hereafter (EP/[OTP][BScB])). Thermogravimetry analysis (TGA) result indicated that the addition of [OTP][BScB] improved the residue yield during thermal degradation. Flammability and combustion tests showed the superior flame-retarding efficiency of the IL. More specifically, the addition of 3 wt% IL made EP/[OTP][BScB] pass the V-0 grade in the vertical burning test (UL-94) and achieve 32.5% value in the limited oxygen index (LOI) test. Cone calorimeter (CC) test showed that, compared with neat EP, EP/10[OTP][BScB] showed a reduction in the peak heat release rate (PHRR) and total heat release (THR) of by 39.7% and 21.8%, respectively, during combustion. Accordingly, the flame-retarding mechanisms in the gas and condensed phases were investigated in detail. In addition, tensile tests showed that the incorporation of the IL enhanced the mechanical property of EP/[OTP][BScB] to some extent. Moreover, UV–vis spectroscopy showed that the transparency of EP was basically maintained on the addition of [OTP][BScB]. Therefore, the IL [OTP][BScB] is a promising flame retardant to improve the properties of EP comprehensively.

KEYWORDS
epoxy, flame retardance, flame-retarding mechanism, ionic liquid

1 | INTRODUCTION

Owing to the concerns about the environment and economy, flame retardants (FRs) for polymer-based materials has stepped into a new era, where perspective research focus on their facile and economic preparation as well as highly efficient and environmentally benign solutions.[1-3] Thanks to their excellent properties, epoxy resins (EPs) have received great attention and have found wide applications in electronic device sealing, construction, aerospace, and so forth.[4,5] However, the inherent flammability limits their use in highly demanding circumstances. Therefore, many halogen-free organic compounds and nanostructured fillers have been used as flame-retardant additives alone or combined with heterogeneous materials as hybrids to improve the flame retardancy of EPs.[6-10] Recently, a few of nanomaterials have shown excellent flame-retarding efficiency; with 3 wt% or even less content, they have achieved self-extinguishment for EP in 10 s in the vertical burning test (UL-94 test, V-0 rating).[11-13] However, the fundamental properties of EP, such as thermal stability, optical property, and mechanical property, are inevitably affected by the addition of FRs. So, how to achieve a desirable

balance between fire retardancy and other properties remains a great challenge.[14]

Ionic liquids (ILs), a class of molten salts, have received much interest because of their unique features such as excellent dissolvability, zero saturated vapor pressure, and nonflammability.[15] To date, the applications of ILs on polymeric material have spanned over a wide range of plasticizers,[16] curing agents,[17] and solvents for polymerization.[18] Room-temperature ionic liquids (RTILs) are a kind of ILs that remain in the liquid state at room temperature and below (even as low as −96°C), and possess desirable viscosity and solubility in a certain temperature range.[15] It is conceivable that RTILs allow polymeric composites to be more homogeneous and promote interfacial adhesion between the host polymer and the additive.

Additionally, ILs are promising FRs because of their tunable chemical structure and highly flexible molecular design of both anions and cations.[19,20] It is widely reported that several flame-retarding elements and groups, such as phosphorous, sulfur, and polyoxometalate cluster, have been introduced into ILs to improve the flame retardancy of EPs. Xiao et al. synthesized imidazole-based ILs containing the phosphite ester to reinforce the fire safety of EPs. Their result showed that the ILs with Br as anion made the EP composites pass V-0 grade in UL-94 test with 4 wt% loading, whereas the EP/IL composite reached same classification with the addition of 6 wt% when phosphomolybdic acid hydrate was the anion of the ILs.[21,22] Shi et al. also prepared phosphorous-functionalized imidazolium ILs [Dmim]Tos by quaternization, by which the EP/[Dmim]Tos composite passed V-0 rating and obtained 32.5% of LOI (limiting oxygen index) value when 4 wt% [Dmim]Tos was added. More importantly, the composites showed negligible influence of [Dmim]Tos on the optical and mechanical properties.[23] Moreover, imidazole-based ILs have the unique advantage that *N*-methylimidazole has potential latent curing behavior for EP, so that the FRs can provide effectiveness at the molecular level.[24,25] On the other hand, IL-based epoxy resins were also prepared by phosphonium curing directly. It is worth noting that phosphonium ILs displayed high reactivity to EP prepolymer when converted to networks, resulting in higher cross-link density compared with a traditional commercial hardener.[26-28] However, the EP composite containing such phosphonium ILs suffered from brittle fracture. Nevertheless, the EP composite with 10 phr IL content still showed significant reduction in the peak value of heat release and total heat release of up to 42.8% and 31.6%, respectively, in a cone calorimeter (CC) test.[29] All in all, the EP composite containing functional ILs showed remarkable enhancement in fire retardancy compared with IL-free EP. However, the fundamental properties of EP/ILs, including thermal stability as well as mechanical and optical properties, easily compromise the improvement in flame retardancy.[30] In addition, there is no publicly available report that EP/ILs pass V-0 rating in the vertical burning test in 3 wt% content, suggesting that the flame-retarding efficiency of ILs needs to be further improved.

Thus, it is natural to think to further explore novel, highly efficient ILs to improve the comprehensive performance of EPs. Similar to phosphorous, boron has been proven to be a dehydrating agent for char formation at high temperatures.[31] Here, an IL with triphenylphosphine as cation and chelated orthoborates as anion, labeled [OTP][BScB], was synthesized and introduced into EP to prepare the EP/[OTP][BScB] composite. The thermal stability and mechanical and optical properties of EP/[OTP][BScB] were investigated. Flame retardancy and the corresponding mechanism of functioning of the EP composite are discussed in detail.

2 | EXPERIMENTAL

2.1 | Materials

The epoxy resin DGEBA (commercial name: E-51) was a product of Jiangsu Sanmu Chemical Reagent Co. Ltd. 4,4-Diaminodiphenyl methane (DDM, 98%), triphenylphosphine (TPP, 99%), 1-bromooctane (98%), lithium carbonate (99%), and salicylic acid (99%) were purchased from Aladdin Industrial Corporation. Boracic acid (98%) was supplied by Sinopharm Chemical Reagent Co. Ltd. Solvents including acetonitrile, ether, and toluene were bought from Shuangshuang Co. Ltd. All reagents were used directly as received without any further purification.

2.2 | Synthesis octyltriphenylphosphonium bromide ([OTP]Br)

At room temperature, 26.2 g (0.1 mol) TPP was dissolved in 70 ml toluene in a 250-ml three-neck flask, and then 12.9 ml (0.12 mol) 1-bromooctane was added. When the system was homogeneous, the mixture was heated at 120°C for 24 h. The mixture was naturally cooled to room temperature and washed with ether several times for removing any raw products. After that, a faint yellow viscous liquid was obtained by drying at 80°C under vacuum overnight.

2.3 | Synthesis of lithium 4,4'-dioxo-4*H*,4'*H*-2,2'-spirobi[benzo[*d*][1,3,2]dioxaborinin]-2-uide (chelated orthoborates lithium, Li [BScB])

The preparation of chelated orthoborates Li[BScB] was according to previous literature.[32] Briefly, in a 250-ml flask equipped with reflux equipment, 1.24 g (20 mmol) boracic acid and 0.74 g (10 mmol) lithium carbonate were dispersed in 80 ml acetonitrile. When temperature reached 40°C, 5.52 g (40 mmol) salicylic acid was slowly added into mixture and the system turned almost transparent. The reaction was carried out at 80°C for 4 h. The mixture was cooled to room temperature for the next preparation.

2.4 | Synthesis of octyltriphenylphosphonium-chelated orthoborate ([OTP][BScB])

Octyltriphenylphosphonium-chelated orthoborate [OTP][BScB] was synthesized by the ion-exchange reaction between [TPB]Br and Li

[BScB]. First, [OTP]Br was dissolved in acetonitrile. Then the mixture was poured into Li [BScB] solution. The molar ratio of [OTP]Br and Li [BScB] was strictly controlled to 1:1.1. The ion-exchange reaction was carried out at 60°C for 6 h. The crude product was obtained by distillation and extraction (dichloromethane and deionized water). The water phase during extraction was tested by aqueous $AgNO_3$ to ensure that it was halogen free. The faint yellow IL [OTP][BScB] was obtained by drying in a vacuum oven at 100°C for 2 days (yield: 98%). The preparation of [OTP][BScB] and the photograph of the IL at room temperature are shown in Scheme 1.

2.5 | Preparation of EP and EP composites

The EP and EP/[OTP][BScB] composites were cured with DDM as the curing agent. The epoxy monomer (100 g) and different wt% of [OTP][BScB] were mixed together and stirred vigorously at 110°C until the mixture was homogeneous. Then, DDM was added to the system and stirred until complete dissolution. The mixture was transferred into a vacuum oven (0.8 Mpa) at 100°C for 3 min to remove bubbles. Afterwards, the mixture was poured into a preheated mold and cured at 120°C for 2 h and 140°C for 2 h, respectively. The blank EP was cured directly without [OTP][BScB]. The samples were named EP, EP/3[OTP][BScB], EP/5[OTP][BScB], and EP/10[OTP][BScB], where the numbers indicate the weight percentage of [OTP][BScB].

2.6 | Characterization

Fourier transform infrared (FTIR) spectra were recorded using a Nicolet 6700 spectrophotometer using KBr pellets. [OTP][BScB] was coated on KBr plates for testing.

NMR spectra was recorded with a Bruker AV400 NMR spectrometer (400 MHz) using $CDCl_3$ as the solvent for [OTP][BScB].

Thermal degradation of the composites was studied by a thermogravimetric analyzer (TGA, NETZSCH, Germany). Samples (7 mg) were heated from room temperature to 800°C at the heating rate of 10°C/min in air and nitrogen atmosphere, respectively. The flow rate of nitrogen was 30 ml/min.

Morphology of the residual char was observed by a scanning electron microscope (SEM, MIRA3,TESCAN, Czech Republic). The samples were sprayed with gold three times.

The vertical burning test (UL-94) was carried out by a burning instrument (FTT 0082, England) according to ASTM D3801, for which the test samples were prepared in the size 130 mm × 13 mm × 3.2 mm.

The samples for the LOI test were of dimensions 100 × 6.5 × 3 mm according to ASTMD 2863, and were measured on an LOI tester (JF-3, Dajia Analytical Instrument Corp., Hebei, China).

The combustion behavior of the composites was characterized by the CC test (CCT, FTT Co., FTTi-cone PLUS) according to ISO 5660 standard. Samples of size 100 × 100 × 3 mm were wrapped in aluminum foils and exposed horizontally to 50 kW/m^2 external heat flux.

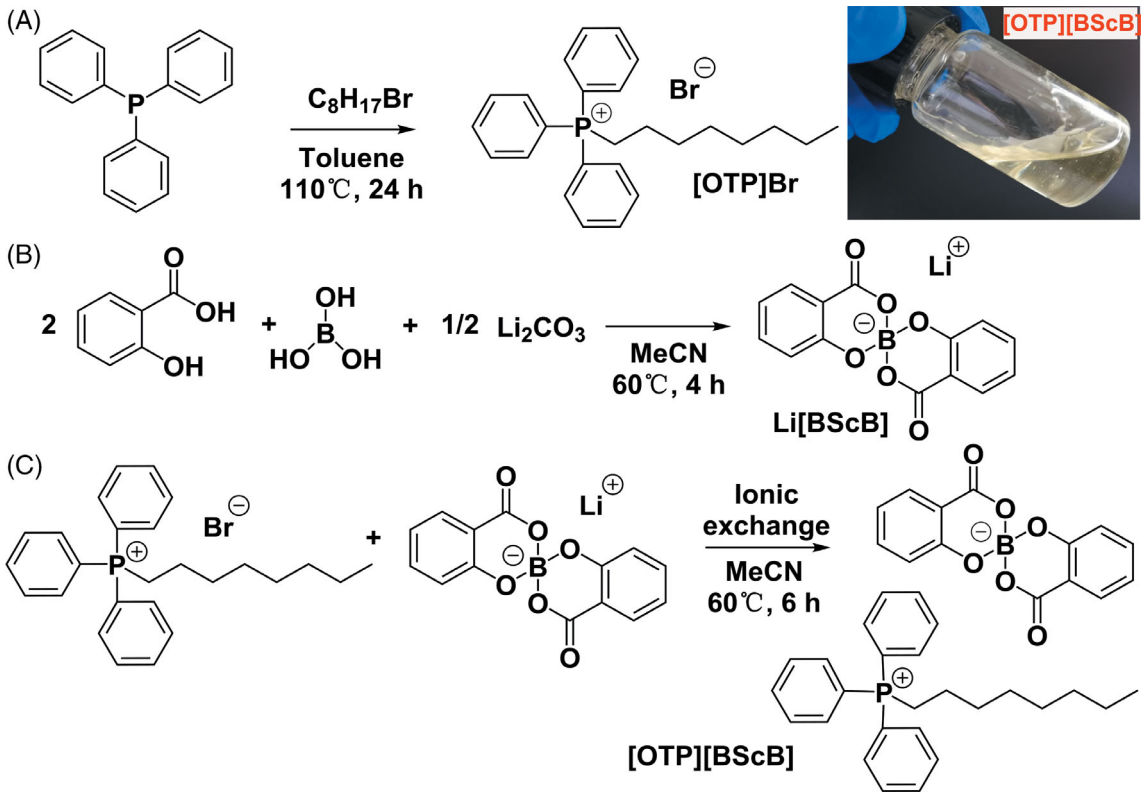

SCHEME 1 Preparation and photograph of the ionic liquid [OTP][BScB]

Raman spectroscopy was performed with a LabAMHR laser Raman spectrometer (S.A.S Co, France.). The excitation wavelength was 325 nm.

X-ray photoelectron spectroscopy (XPS) of the residual char was performed using an ESCALAB 250Xi (ThermoFisher Scientific company) instrument.

Thermogravimetric analysis/infrared spectrometry (TG-FTIR) of the samples was performed on the TGA Q5000 IR thermogravimetric analyzer coupled to the Nicolet 6700 FTIR spectrophotometer. The weight of the samples was 7 mg, and the sample was heated from 50 to 800°C at a heating rate of 10°C/min under nitrogen atmosphere with a flow rate of 30 ml/min.

Py-GC-MS (pyrolysis-gas chromatography-mass spectrometry) was carried out on a GC-TOF-MS system (DANI, Italy) coupled with a CDS5200 pyrolyzer (CDS, USA). The samples were heated from 50 to 600°C at the rate of 1000°C/s in helium atmosphere and maintained for 20 s. The heating program of the capillary column was as follows: 50°C for 2 min, then increased to 350°C at the rate of 15°C/min and maintained at 350°C for 5 min. The mass spectral data were analyzed using the NIST library.

Tensile tests were conducted on a computer-controlled electronic universal testing machine (WDW-20,Jinan Heng Rui Jin Testing Machine Co. Ltd, China).The sample size was 100 × 10 × 4 mm for the tensile test according to GB/T 1040.2–2006 at the speed of 10 mm/min. Each specimen was tested five times and the average value was taken.

The glass transition temperatures (T_g) of the EP composites were recorded on a DSC-7 instrument (Pechino Elmer company, USA). Samples were heated from 80 to 250°C at a rate of 10°C/min in nitrogen atmosphere.

Ultraviolet–visible (UV–vis) spectra of the EP composites were recorded on a spectrometer (Model UV-2102PC, UNICO). The thickness of the samples was 3 mm.

3 | RESULTS AND DISCUSSION

3.1 | Characterization of [OTP][BScB]

Nuclear magnetic resonance spectroscopy was used to establish the chemical structure of the IL [OTP][BScB]. From the ^{1}H-NMR spectra in Figure 1A, the peak at 0.65 ppm was attributed to the methyl hydrogen at the end of the aliphatic chain, the signal at 3.09 ppm was assigned to methylene linked with phosphorous,, and the chemical shift range 0.97–1.41 ppm belonged to the alkyl group in the cation. Hydrogens in the aromatic ring of both cation and anion exhibited their corresponding chemical shifts in range 6.62–7.64 ppm. Figure 1B shows that there is a single peak at 19.4 ppm in the ^{31}P-NMR spectrum, implying only one phosphorous atom in the structure. The results of NMR indicate that chemical structure of as-prepared IL [OTP][BScB] is consistent with the structure in Scheme 1.

The chemical structure of [OTP][BScB] was also characterized by FTIR, as shown in Figure 1C. In the FTIR spectrum, the peaks belonging to the alkyl group appear in range 3066–2867/cm and those of the aromatic ring at 1606, 865, and 754/cm The peak at 1698/cm is ascribed to the COOH bond, and the characteristic peaks of P—C and B—O were at 1436 and 1315/cm, respectively. Based on above results, it was confirmed that the IL [OTP][BScB] was prepared successfully.

The thermal degradation behavior of [OTP][BScB] was investigated by TGA in air and nitrogen atmospheres. The IL underwent a multistep thermal decomposition in both air and nitrogen, as shown in Figure 1D. The decomposition of ILs indicated that the temperature of initial decomposition (temperature corresponding to 5 wt% mass loss) was 316°C in nitrogen and 334°C in air atmosphere, and the first decomposition stage was eventually completed at 403°C in both atmospheres, whereas the mass loss reached 17 wt% in nitrogen and 18 wt% in air atmosphere. The initial decomposition in both atmospheres was caused by the degradation of the alkyl chain in the structure (analysis using TG-FTIR). Subsequently, the IL displayed the main decomposition in nitrogen with about 76 wt% mass loss in the temperature range 403–503°C, while the second decomposition of IL in air ended early at 468°C, involving 70 wt% mass loss. The decomposition of the chemical structure of the IL occurred in this region. The third stage of decomposition in air occurred in the range 468–682°C, accompanied by 8 wt% mass loss, which was attributed to the decomposition of residues due to thermal oxidation. Finally, the residual yield was 5.8 wt% in nitrogen and 3.1 wt% in air atmosphere. Compared to the thermal stability results of ILs as flame retardants in previous works, [OTP][BScB] had higher decomposition temperature.[21-23] It suggests that [OTP][BScB] is a promising flame retardant additive to meet many polymer processing schemes due to the overlap of the decomposition temperatures of the polymer matrix and the flame retardant.[3]

3.2 | Thermal stability of EP and EP composites

Thermal stability of EP and EP composites in air and nitrogen atmospheres was investigated by TGA. The curves of TG and DTG are shown in Figure 2 and the related data are given in Tables 1 and 2.

The temperature corresponding to 5 wt% mass loss ($T_{5\%}$) was defined as temperature of initial decomposition. With the IL incorporated into the EP matrix, the $T_{5\%}$ of the composites decreased as the content increased in both atmospheres. This behavior is caused by the breakage of the alkyl chain of [OTP][BScB] (analysis in TG-FITR section). After that, the TGA curves displayed two shoulders in air atmosphere but only one decomposition region in nitrogen atmosphere. For degradation in air, the first stage is attributed to the thermal decomposition of the polymer chain, and the second region is ascribed to the thermal oxidation decomposition of the residues.[23] During the multistep decomposition, the temperature at maximum mass loss rate (marked as T_{max}) of all EP/[OTP][BScB] showed a value (T_{max1}) similar to that of EP in first decomposition stage but a slight reduction in T_{max2} in second decomposition stage with increased IL content. The peak value of DTG of EP/[OTP][BScB], representing the maximum mass loss rate (MMLR), obviously reduced in first decomposition region ($MMLR_1$) but showed an almost similar value in $MMLR_2$

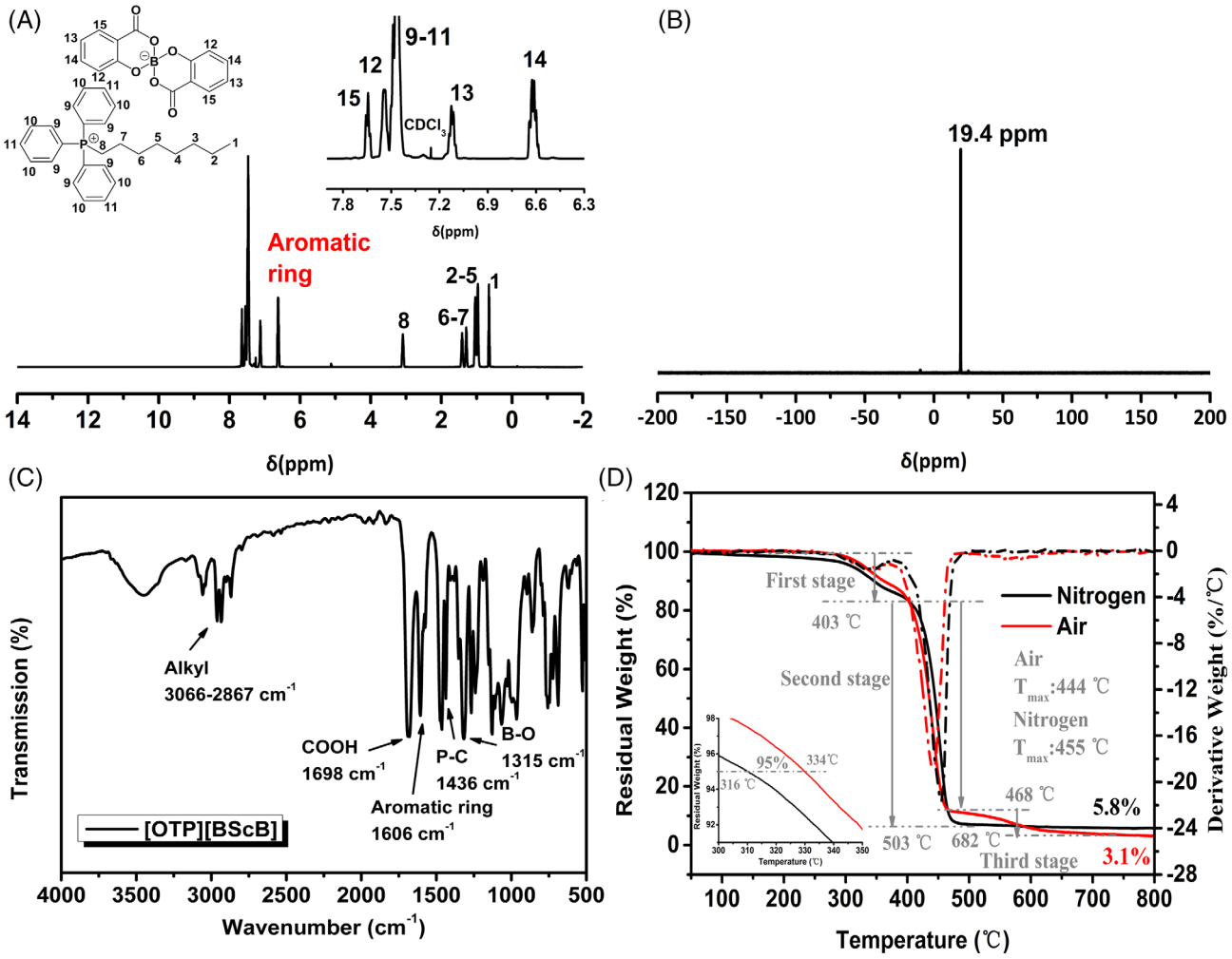

FIGURE 1 (A) ^{1}H-NMR, (B) ^{31}P-NMR, (C) FTIR spectrum, and (D) TGA curves of [OTP][BScB]

in second decomposition, compared to EP, indicating that the addition of the IL alleviated the thermal degradation of the polymer chain but was unable to impact the thermal oxidation. With the temperature rising to 800°C, EP and EP/3[OTP][BScB] showed nearly zero char yield, while it reached 1.5 wt% and 2.5 wt% with 7 wt% and 10 wt% loading.

During thermal decomposition in nitrogen atmosphere, EP/[OTP][BScB] composites also showed a lower $T_{5\%}$ but their T_{max} shifted to a higher value. Besides, the MMLR of EP/[OTP][BScB] showed a more visible reduction than EP, implying a slower pyrolysis rate. In addition, the char yield at 800°C in nitrogen showed a similar trend as in air, with EP/7[OTP][BScB] and EP/10[OTP][BScB] giving more residual yield than EP and EP/3[OTP][BScB]. The increased char yield at high temperature was because the aromatic flame retardants induced the formation of a large quantity of thermo-stabilization products; meanwhile, the generated phosphate species also enhanced the thermal stability of the residues.[33,34]

The T_g values of EP composites are also given in Table 2. T_g was 147°C for EP, 146°C for EP/3[OTP][BScB], 134°C for EP/7[OTP][BScB], and 129°C for EP/10[OTP][BScB]. Although a rigid chemical structure existed in [OTP][BScB], the presence of the alkyl chain may contribute to [OTP][BScB] to be used as a plasticizer for thermosetting EP.[9]

3.3 | Flammability of EP and EP composites

The flammability of EP and EP/[OTP][BScB] was analyzed by LOI and the vertical burning test (UL-94). From the picture of EP and EP composites after LOI test in Figure 3A, it can be seen that all samples retained decent transparency; meanwhile, they generated a carbonaceous residue after burning. In addition, the LOI value of neat EP was 26.3 ± 0.5%, whereas all EP/[OTP][BScB] composites had much higher values than EP, as shown in Figure 3. For instance, the LOI value of EP/3[OTP][BScB] dramatically improved to 32.4 ± 0.4%, which is 18.2% more than that of EP. From the UL-94 results, it can be seen that all EP/[OTP][BScB] samples exhibited self-extinguishing behavior in 10 s after ignition, whereas neat EP displayed sustained burning, suggesting that [OTP][BScB] made EP composites to pass V-0 rating. To show this clearly, the vertical burning process of EP/3

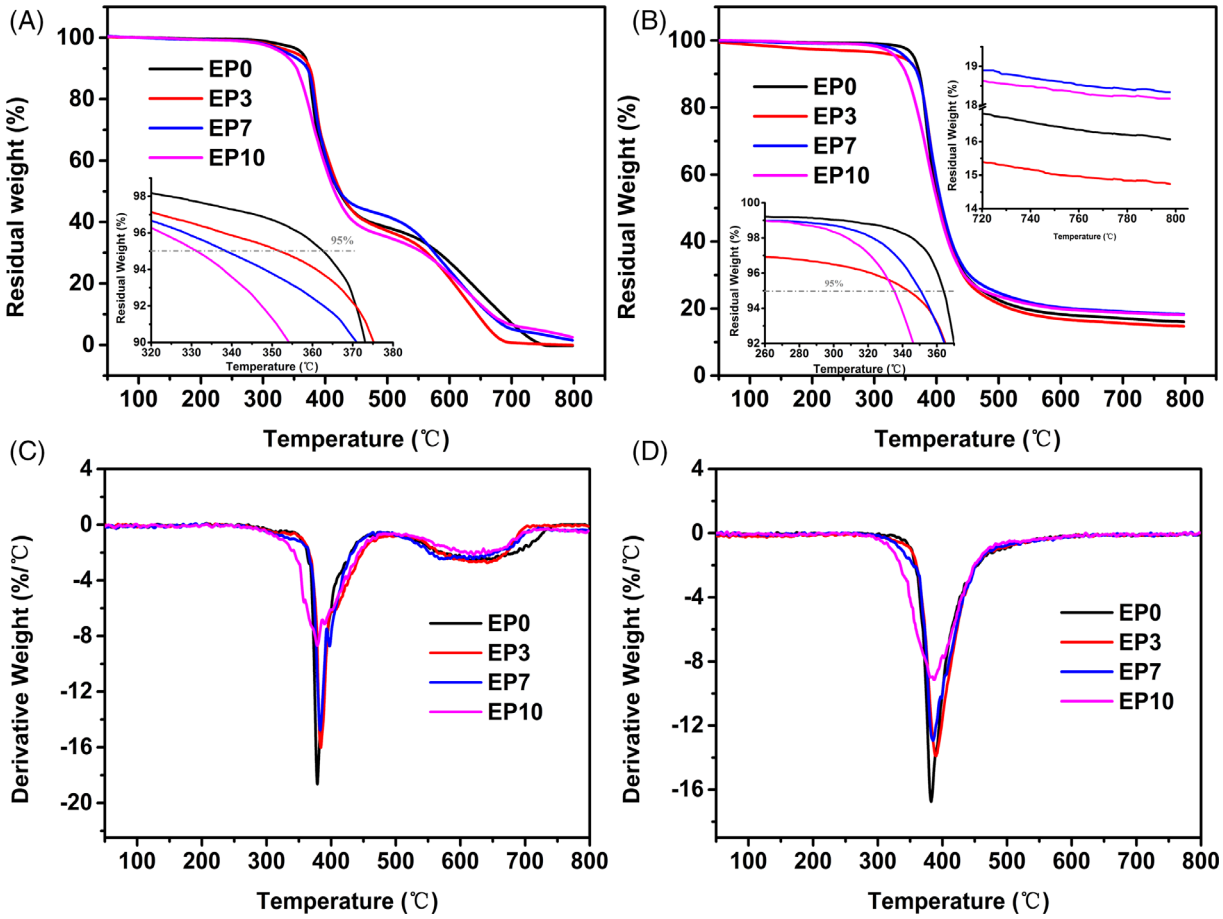

FIGURE 2 TG and DTG curves of EP and EP composites (A,C) in air and (B,D) in nitrogen atmosphere

TABLE 1 TGA results of EP and EP composites in air atmosphere

Sample	$T_{5\%}$ (°C)	T_{max} (°C)		MMLR (%/°C)		Char yield at 800°C (%)
		T_{max1} (°C)	T_{max2} (°C)	$MMLR_1$	$MMLR_2$	
EP	365	379	626	−18.6	−2.6	0
EP/3[OTP][BScB]	358	383	630	−16.0	−2.6	0
EP/7[OTP][BScB]	344	383	568	−14.8	−2.5	1.5
EP/10[OTP][BScB]	335	379	612	−8.6	−2.1	2.5

TABLE 2 TGA and DSC results of EP and EP composites in nitrogen atmosphere

Sample	$T_{5\%}$ (°C)	T_{max} (°C)	MMLR (%/°C)	Char yield at 800°C (%)	T_g (°C)
EP	365	383	−16.7	16.1	147
EP/3[OTP][BScB]	350	390	−13.9	14.7	146
EP/7[OTP][BScB]	353	385	−13.0	18.3	134
EP/10[OTP][BScB]	337	388	−9.1	18.2	129

[OTP][BScB] after two ignitions is displayed in Figure 3C, where the flame extinguished in 3 and 5 s, respectively. The self-extinguishment and the increase of LOI correspond to ignition behavior depended not only on the condensed-phase flame retardant ability but also on more actions in the gaseous phase, such as radical scavenging and diluting combustible volatiles.[25,35-37] As a phosphorus-containing IL, the probable reason was the generation of active gaseous P species during burning.[23] All in all, EP/[OTP][BScB] demonstrated promising flame retardancy even in low content, suggesting that [OTP][BScB] had a highly efficient flame retarding ability.

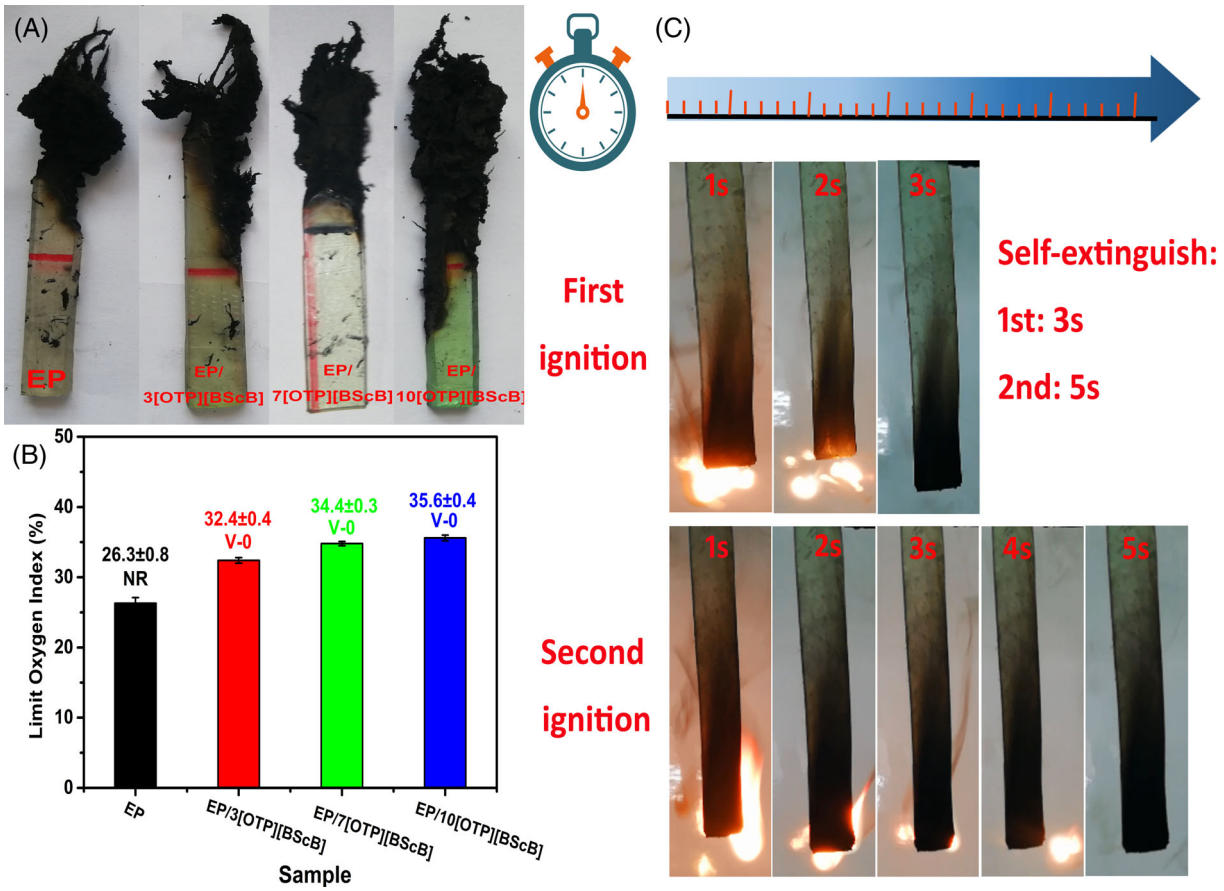

FIGURE 3 (A) Digital photograph of samples after LOI test. (B) Results of LOI and UL-94 test and (C) vertical burning process of EP/3[OTP][BScB]

3.4 | Combustion behavior of EP and EP composites

The CC test is an effective bench-scale method to estimate the combustion behavior of polymeric material in a developing fire scenario.[37] The heat release and smoke production of EP composites during combustion versus time are plotted in Figure 4. The related data, including time to ignition (TTI), peak value of heat release rate (PHRR), peak value of smoke production rate (PSPR), total value of heat release (THR) and smoke production (TSP), and effective heat of combustion (EHC) are reported in Table 3.

From Table 3, we can see similar results for the time to ignition for EP and EP/[OTP][BScB], which suggests that [OTP][BScB] hardly has any influence on the ignition behavior of EP. After ignition, neat EP burned rapidly and showed a narrow peak in the HRR curve, indicating typical non-charring performance during combustion. In comparison, a shoulder appeared before PHRR in the curves of EP/[OTP][BScB], corresponding to a steady-state HRR (quasi-static HRR).[9] The shape of the HRR curve (before PHRR) indicates that the addition of ILs brought about a transformation from typical non-charring EP into intermediate thick non-charring EP/[OTP][BScB],[37] afterward, the decomposition of the protective char resulted in further heat release contributing to the peak value. The PHRR and THR at 500 s of EP was 1243 kW/m^2 and 88.4 MJ/m^2, respectively, as shown in Figure 4A,B. With the incorporation of the IL, the PHRR and THR of EP/[OTP][BScB] showed a decreasing trend. For example, the PHRR and THR of EP/10[OTP][BScB] reduced to 749 kW/m^2 and 69.0 MJ/m^2, respectively, which is a decrease of 39.7% and 21.8% compared with those of EP. Besides, all samples exhibited a weak peak in HRR curves at around160–250 s, which is attributed to further thermal oxidation of the surface of residual char. Accordingly, the THR curves gradually increased after 250 s. Furthermore, to evaluate fire safety of the composites, the fire growth rate (FIGRA) and fire performance index (FPI) were calculated.[38,39] It was clearly seen that the FIGRA of EP/[OTP][BScB] decreased but the FPI increased as the [OTP][BScB] content increased, indicating better fire safety of the EP composite in presence of [OTP][BScB]. Therefore, the addition of [OTP][BScB] effectively inhibited or slowed down fire spread and decreased the fire load of EP.

Figure 4C,D shows more details about the smoke production during combustion. As can be seen, the shape of the SPR curves of EP and EP/[OTP][BScB] is similar to that of the HRR curves. EP had PSPR and TSP of 0.44 m^2/s and 30.0 m^2, respectively. By contrast, the corresponding values for EP/3[OTP][BScB] dropped to 0.33 m^2/s and 25.4 m^2, respectively. However, the increase in content of ILs made EP/[OTP][BScB] composites release more smoke, as the TSP of

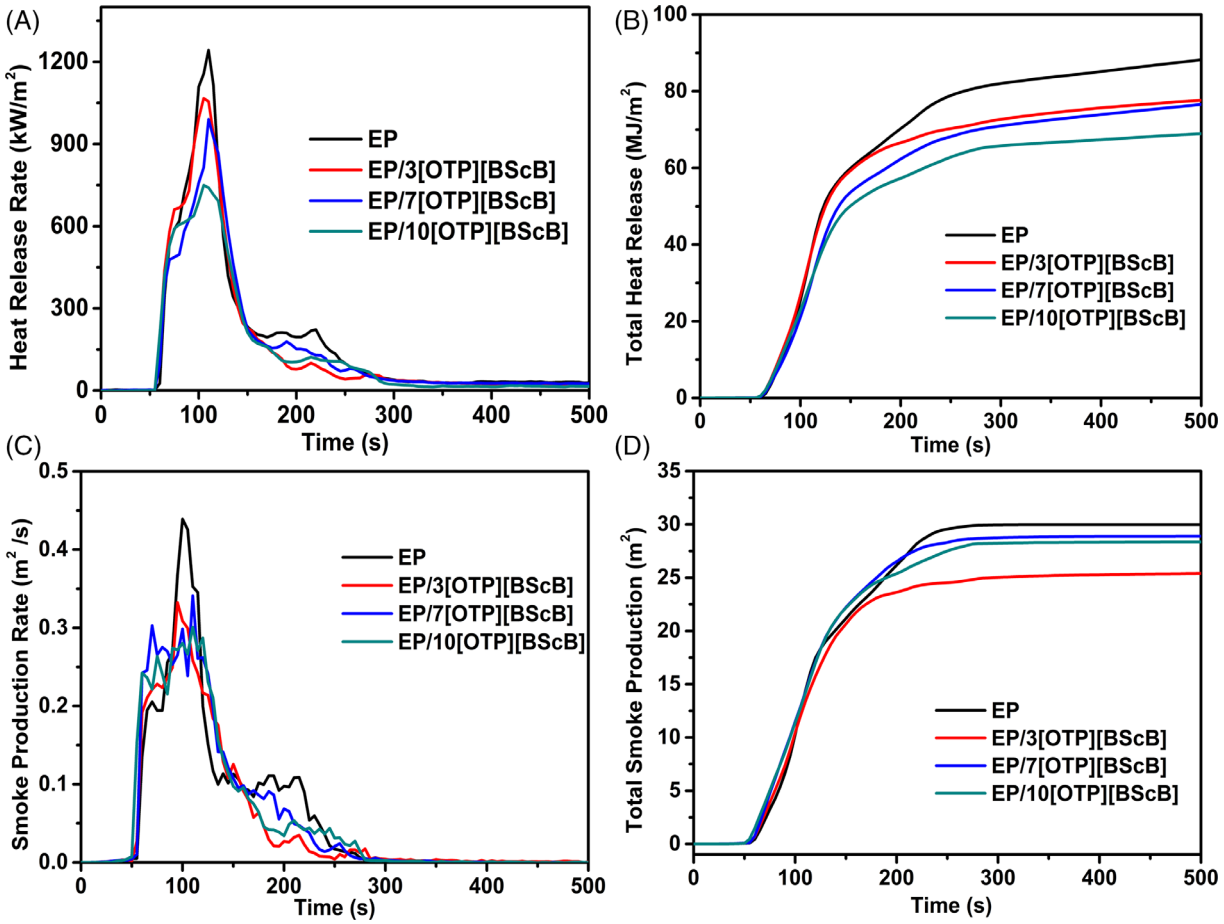

FIGURE 4 (A) HRR, (B) THR, (C) SPR, and (D) TSP curves of EP and EP composites

TABLE 3 Results of cone calorimeter test of EP and EP composites

	EP	EP/3[OTP][BScB]	EP/7[OTP][BScB]	EP/10[OTP][BScB]
TTI (s)	57	55	56	53
PHRR (kW/m^2)	1243	1067	990	749
TTPHRR (s)	110	105	110	105
THR (MJ/m^2)	88.2	77.7	76.6	69.0
PSPR (m^2/s)	0.44	0.33	0.34	0.30
TSP (m^2)	30.0	25.4	28.9	28.4
av-EHC(MJ/kg)	24.8	20.0	24.1	18.6
FIGRA (kW/m^2·s)	11.3	10.2	9.0	7.1
FPI*10^2 (m^2·s/kW)	4.6	5.2	5.7	7.1

EP/[OTP][BScB] with 7 wt% and 10 wt% was higher than that of EP/3[OTP][BScB]. This was probably due to the decomposition of residual char at around 160–250 s, resulting in the production of more smoke particles (TSP curves of EP/7[OTP][BScB] and EP/7[OTP][BScB] show a visible increase in this region). Fortunately, the TSP of all EP/[OTP][BScB] combinations shows a reduction with respect to EP. This result suggests that [OTP][BScB] plays a smoke suppressor role during combustion. In addition, the EHC values of all EP/[OTP][BScB] composites was lower than that of EP, implying the generation of fewer combustible products in the gas phase.

In summary, the IL [OTP][BScB] worked as a flame retardant, resulting in the suppression on heat release and smoke production during combustion.

3.5 | Analysis in the condensed phase

The flame-retarding mechanism of [OTP][BScB] in the condensed phase was investigated by analyzing the morphology, degree of graphitization, and chemical components of the char residue after the CC test.

Figure 5 displays digital photographs of the residual char. Neat EP shows a loose residue after burning, while all EP/[OTP][BScB] composites formed dense residual blocks and their surface became compact as the [OTP][BScB] content increased, implying good physical barrier of the residual char.

Scanning electron microscopy (SEM) was employed to provide insights into the morphology of the residual char. The exterior and interior morphology of residual char of EP/[OTP][BScB] composites is shown in Figure 6. The EP residue consists of irregular blocks with distributed cracks and holes. With the addition of 3 wt% and 7 wt% IL, the exterior residues became more compact, but the interior residues still exhibited a porous structure. As the content of ILs was increased to 10 wt%, residues of both sides displayed a smooth and compact surface. Especially for the exterior char layer, the prominent protective and isolative role prevented oxygen and heat permeation into the interior and inhibited the diffusion of pyrolysis products of the substrate as fuel to feed the fire zone. Additionally, energy dispersive spectroscopy (EDS) mapping of the exterior residual char is shown in Figure S1. For EP and EP/[OTP][BScB], the residual char contained the elements carbon, nitrogen, and oxygen, but additionally phosphorus and boron elements existed in the residue of EP/[OTP][BScB]. The elemental masses in the exterior surface of the residues are listed in Table S1. As the content of ILs increased, the mass of C decreased while that of P and B increased, suggesting accumulation and migration of flame-retarding elements in the exterior char residue during combustion. Besides, the SEM photograph and EDS results of the product of phosphorus oxide catalyzing the char formation are shown in Figure S2 and Table S2, evidencing the role of P as a flame retardant in condensed phase. The SEM and EDS results indicate that the decomposed products of [OTP][BScB] participated in char formation and made the residual char compact.

Raman spectroscopy was used to investigate the degree of graphitization of the residual char. As shown in Figure 7, there were two conspicuous peaks at 1360/cm (D peak) and 1590/cm (G peak),

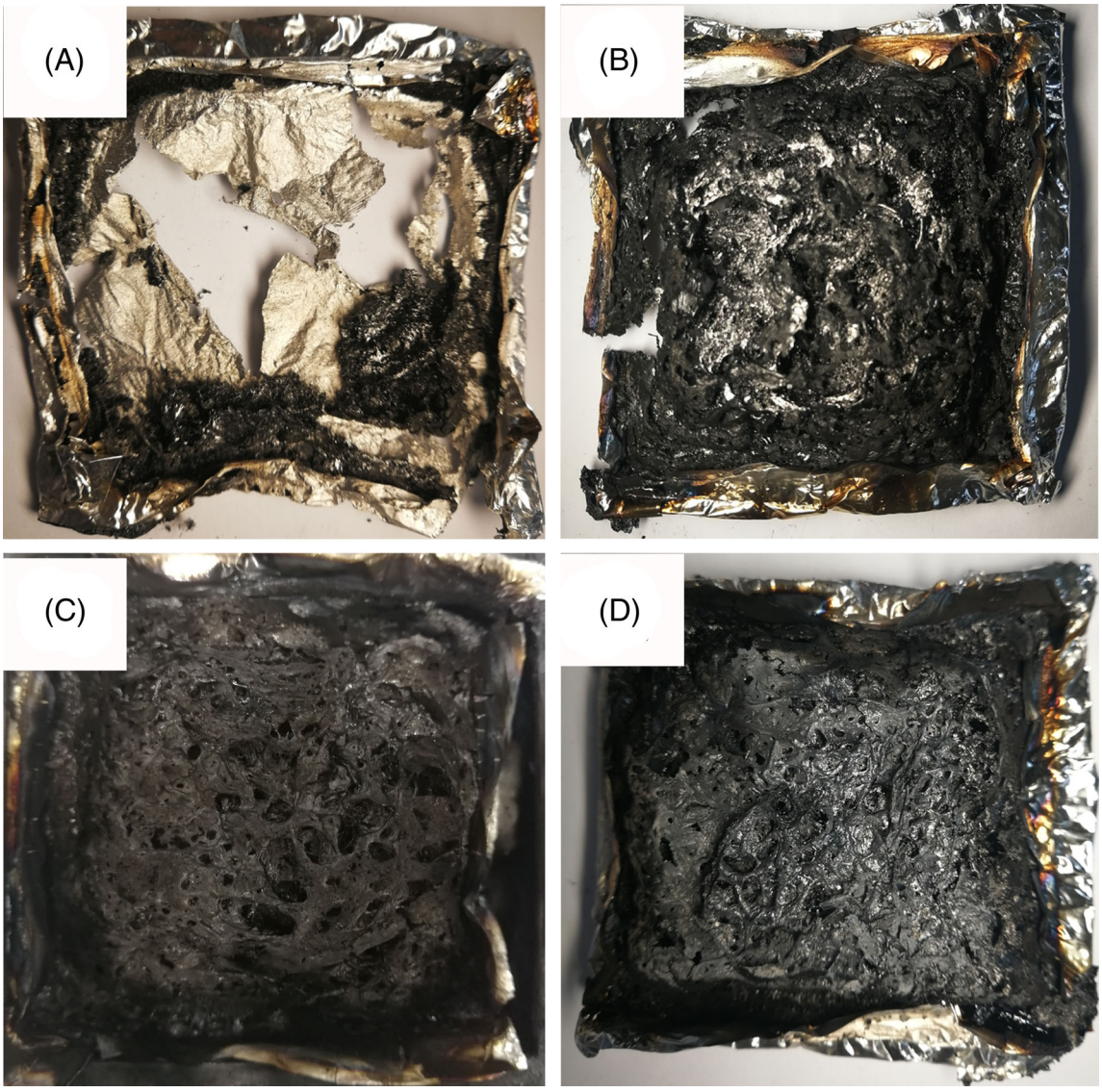

FIGURE 5 Digital photos of the residual char of (A) EP, (B) EP/3[OTP][BScB], (C) EP/7[OTP][BScB], and (D) EP/10[OTP][BScB]

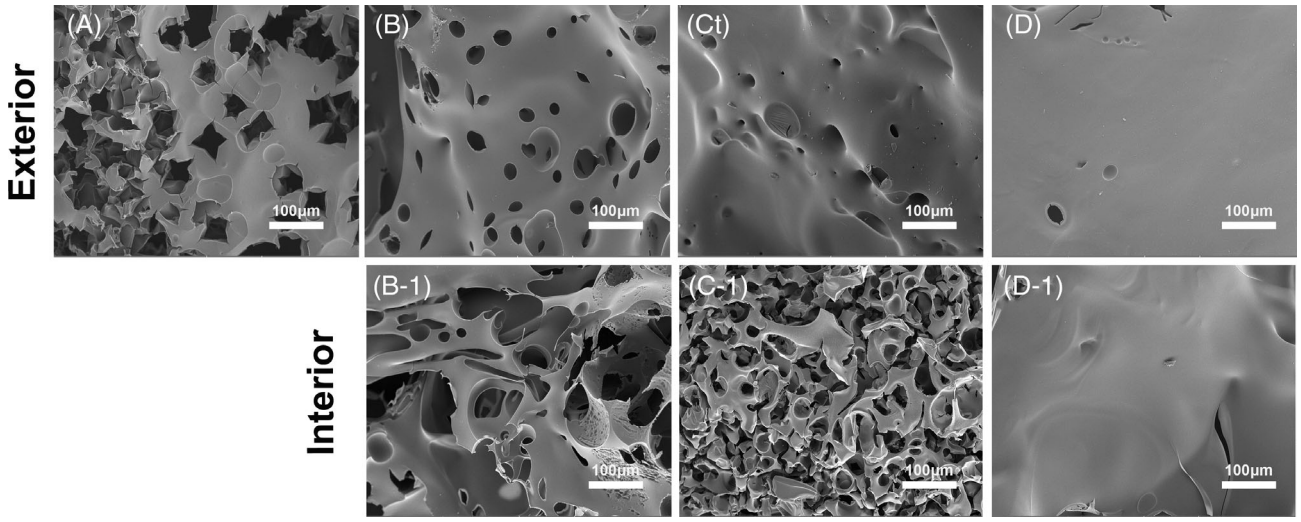

FIGURE 6 SEM photograph of the residual char of (A) EP, (B,B-1) EP/3[OTP][BScB], (C,C-1) EP/7[OTP][BScB], and (D,D-1) EP/10[OTP][BScB]

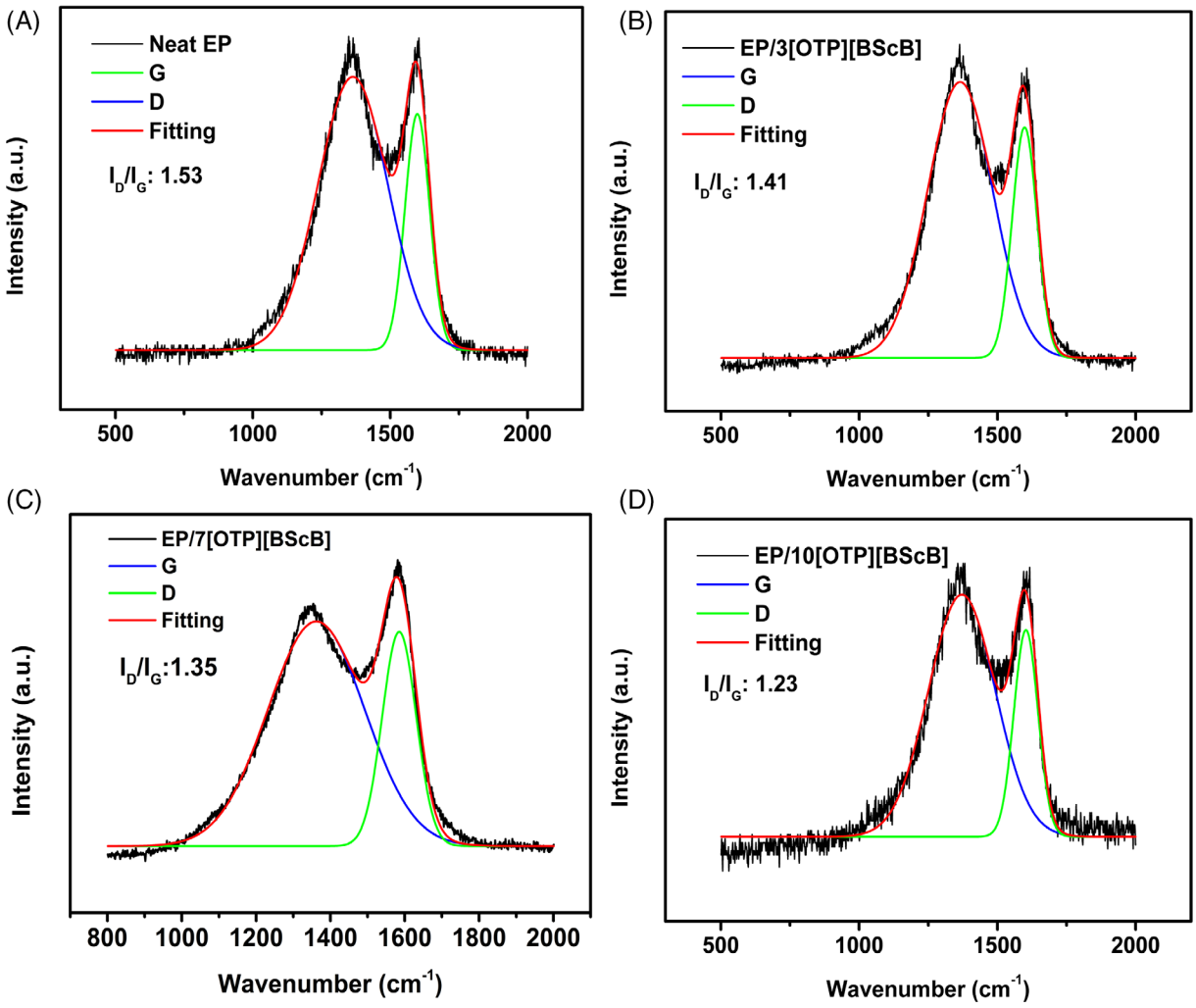

FIGURE 7 Raman curves of the residual char of (A) EP, (B) EP/3[OTP][BScB], (C) EP/7[OTP][BScB], and (D) EP/10[OTP][BScB]

where the D peak represents carbon atoms in a disordered structure and the G peak represents organized carbon. The ratio of areas of the D peak and G peak is denoted as I_D/I_G, a lower value of which represents a higher degree of graphitization. As can be seen, EP has I_D: I_G = 1.53, whereas the value for all EP/[OTP][BScB] samples were lower than that resulting from the rich aromatic chemical structure and catalysis effect of [OTP][BScB]. The Raman results indicate that introduction of [OTP][BScB] has contributed to the increase in the graphitization of the char layer, which provided a better protective shield for the polymer.

To better understand the chemical reaction in the condensed phase during combustion, FTIR and XPS were employed for analyzing the chemical components of the residual char from CC test. From the C 1s spectra of EP and EP composites, three curves corresponding to C—C or C═C bond (284.6 eV), C—OH bond (286.1 eV), and COOH bond (288.1 eV) are found, as shown in Figure 8A–D. The C—C or C═C bond comes from aliphatic or aromatic carbons and the C—OH and COOH bonds are from oxidized carbon, where C_a is used to represent the integral area of C—C or C═C bond and C_{ox} for C—OH and COOH bonds.[40] The value of C_{ox}/C_a reflects the proportion of aromatic carbons in residual char.[41] In our case, C_{ox}/C_a was 1.04 for EP and ~0.4 for all EP/[OTP][BScB] composites. The smaller ratio of C_{ox}/C_a represents a larger concentration of aromatic carbons in the residual char. This means that [OTP][BScB] made EP to produce more aromatic carbons as a protective shield, which is in accordance with the higher graphitization as deduced from the Raman experiments. Actually, this is due to the promotion of P and B derivatives to dehydration in char formation. In addition, Figure 8E shows two peaks in the B spectrum, which is attributed to H_3BO_3 (193.4 eV) and borate (192.2 eV). The existence of boron derivatives indicates that boron evolved into H_3BO_3 and served as an acidic source to participate in char formation. Besides, representative peaks of the addition compounds (P—O—C) and polyphosphate appear at 132.4 and 133.1 eV in the P 2p spectrum, as shown in Figure 8F. These typical acidic products from [OTP][BScB] effectively increased the quantity and improved the compactness of the residues during combustion and thereby directly the enhanced the protective effect of char layer.

From the FTIR spectra in Figure 8G, both EP and EP/[OTP][BScB] exhibit the same absorption peaks of —OH (3425/cm) and C═C in aromatic ring (1608/cm). Apart from these, there are two unique peaks at 1388 and 1257/cm in the spectrum of EP/[OTP][BScB], which are ascribed to B—O and P—O bonds, respectively. This is also evidence that [OTP][BScB] generates phosphate and borate compounds during combustion to catalyze the polymeric matrix to form compact residues.

3.6 | Analysis in the gaseous phase

The self-extinguishing behavior of EP/[OTP][BScB] composites in the vertical burning test implies the possible flame-retarding role in the gas phase, especially for capturing free radicals to interrupt burning by the generated gaseous phosphorus-containing species. Here, the evolved gaseous composition during thermal degradation was analyzed by coupling thermogravimetry with FTIR spectrometry.[42]

In Figure S3A, the Gram–Schmidt curves show lower total absorbance of EP/10[OTP][BScB] than EP, suggesting less gaseous compounds released in the presence of [OTP][BScB] during thermal degradation. Furthermore, the detailed evolution of gaseous products of EP and EP/10[OTP][BScB] versus temperature in nitrogen atmosphere is shown in Figure 9. On comparing the FTIR spectra of EP (A) and EP/10[OTP][BScB] (B), similar characteristic peaks are seen, which belong to water or phenol (3650 and 1257/cm), aromatic compounds (3067, 1495, 822, and 763/cm), hydrocarbons (2972/cm), and ether (1179/cm). Moreover, there is a remarkable difference in the FTIR spectrum of EP/10[OTP][BScB] in that an absorption peak appears at 1114/cm (red arrow), which is ascribed to the stretching vibration of P—Ar or P—O bond.[9,43]

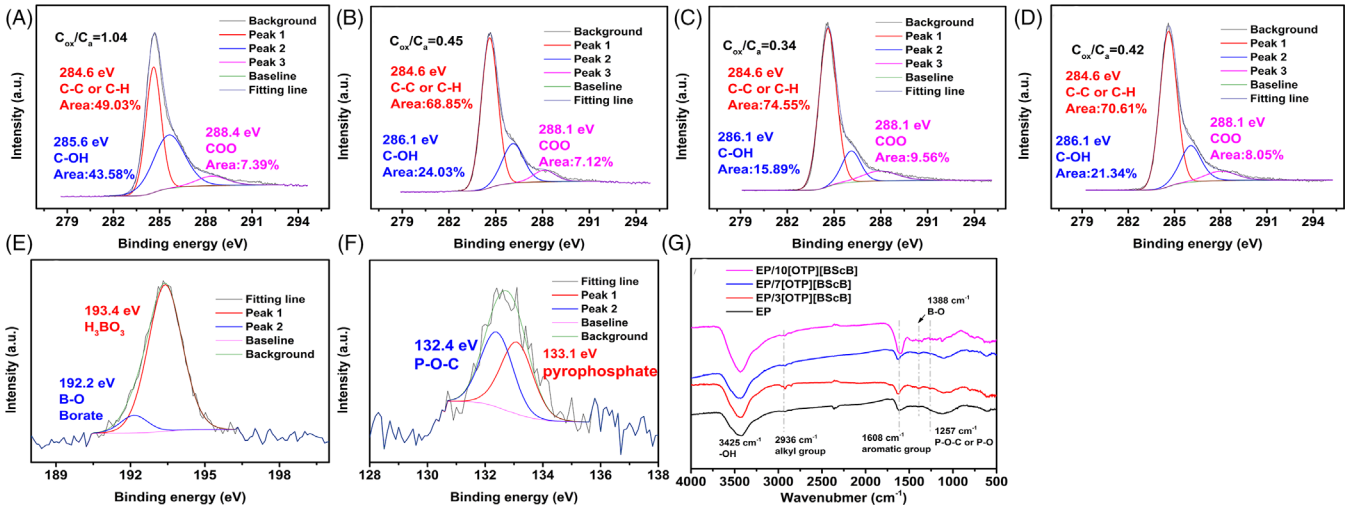

FIGURE 8 XPS spectra the residual char: (A) C 1s of EP, (B) EP/3[OTP][BScB], (C) EP/7[OTP][BScB], and (D) EP/10[OTP][BScB]. (E) B 1s and (F) P 2p spectra. (G) FTIR spectra

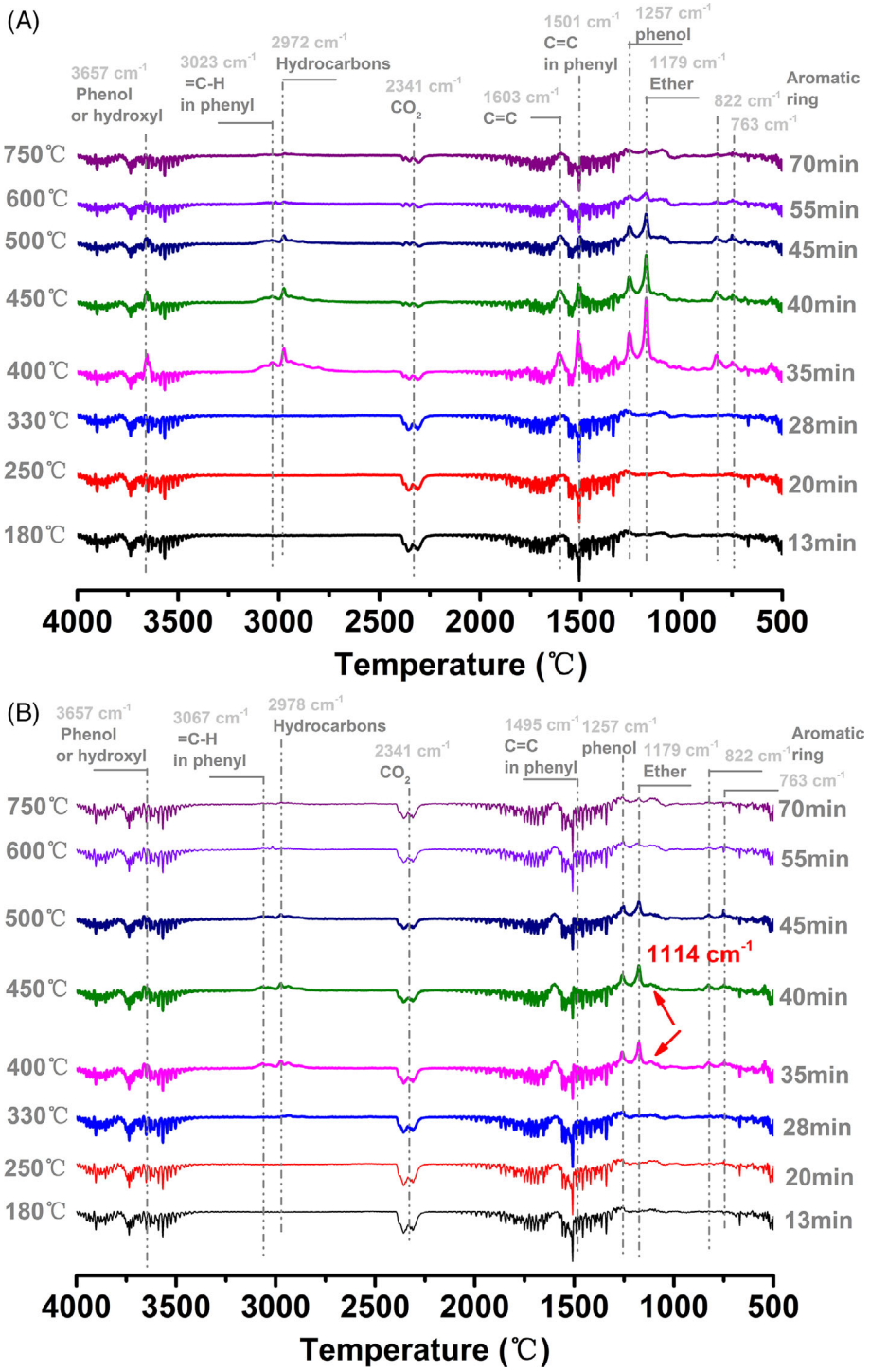

FIGURE 9 TG-FTIR spectra of the pyrolysis products for (A) EP and (B) EP/10[OTP][BScB]

To study the changes of the evolved gaseous products versus various temperatures more clearly, the FTIR spectra at 330°C, $T_{5\%}$, and T_{max} are shown in Figure S3B–D, respectively. As can be seen, only EP/10[OTP][BScB] released alkene compounds at 330°C, evidencing that the preceding decomposition of the EP/[OTP][BScB] composite was caused by the breakage of the alkyl chain. At $T_{5\%}$, EP initially generated alkyl- and ether-based compounds. With temperature increasing to T_{max}, EP/[OTP][BScB] released additional phosphorous species, suggesting the flame-retarding role the ILs exerted during the main decomposition.

To further analyze the gaseous phosphorous species the ILs released and to understand the mode of flame-retarding action of [OTP][BScB] in the gaseous phase during combustion, the pyrolysis behavior of [OTP][BScB] and EP/[OTP][BScB] was analyzed by py-GC-MS. The total-ion chromatograms and mass spectra of the main phosphorous species are shown in Figure 10. The possible chemical structures of the primary pyrolysis fragments are summarized in Tables S3 and S4 in detail.

In Figure 10A, the decomposition products of the alkyl chain of [OTP][BScB] were alkane (*m/z* = 44, 45, and 56) and benzene (*m/*

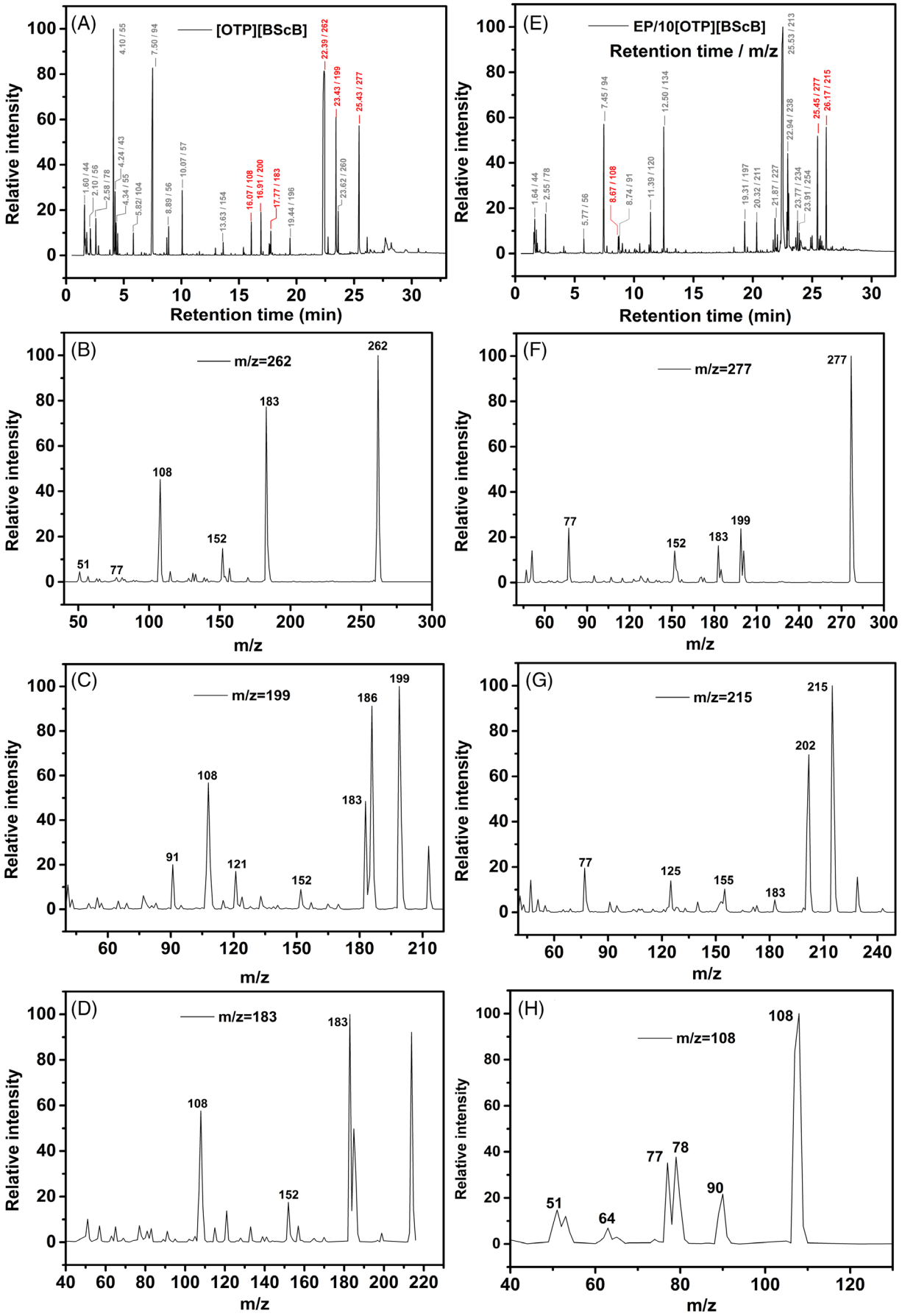

FIGURE 10 py-GC-MS results of the main gaseous products of (A) total-ion chromatograms of [OTP][BScB] and (B–D) mass spectra of *m/z* = 262, 199, and 183. (E) Total-ion chromatograms of EP/10[OTP][BScB] and (F–H) mass spectra of *m/z* = 277, 215, and 108. Red mark indicates phosphorus-containing species

z = 77) species. Besides, some phosphorous-containing fragments (marked red) also emerged as a result of the decomposition of the cation, whose *m/z* values were 108, 200, 183, 262, 199, and 277, respectively. Part of the mass spectra of the fragments and their possible decomposition routes are shown in Figure S4 and Scheme S1. Furthermore, the mass spectra of triphenylphosphine (*m/z* = 262) and of other main pyrolysis products (*m/z* = 199 and 183) are shown in Figure 10B–D. It is worth noting that the all these species possessed same fragment of *m/z* = 108; meanwhile, [OTP][BScB] also directly released this fragment during pyrolysis. In fact, the fragment, a kind of organophosphinidene, is a stable free radical (C_6H_5P, phenylphosphinidene) in the gas phase.[44] It can be deduced reasonably that phenylphosphinidene may be contributing to the formation of other phosphorous-containing fragments such as those of *m/z* = 183 and 199, and indirectly participating in the establishment of the fragment of *m/z* = 277 by a multistep addition and rearrangement of the aromatic radical. In addition, the anion of [OTP][BScB] also released xanthen-based (*m/z* = 196) and ketone-based (*m/z* = 260) species and further evolved into a phenol fragment (*m/z* = 94). The decomposition process of [OTP][BScB] is displayed in Scheme 2A.

The epoxy resin cured by 4,4-diaminodiphenyl methane released phenol (*m/z* = 94), bisphenol-A (*m/z* = 213), phenylamine compounds (*m/z* = 198), etc. during pyrolysis.[23] These fragments also can be found in the total-ion chromatograms of EP/10[OTP][BScB]. Besides, as [OTP][BScB] is incorporated into EP, the EP composite also released phosphorous-based species with *m/z* values 215, 277, and 108, as shown in Figure 10F–H. The fragments of *m/z* = 277 and 108 surly came from the decomposition of [OTP][BScB], but the fragment of *m/z* = 215 was present only in the decomposition of EP/[OTP][BScB] composites. Where did this additional fragment come from? Based on the mass spectrum, the evolution of the fragment is depicted in Scheme 2B. It is probable that phenylphosphinidene in combination with the OH free radical (*m/z* = 17) produced the fragment of *m/z* = 125, which further reacted with phenyl (*m/z* = 77) and methane (*m/z* = 14) free radicals to generate the fragment of *m/z* = 216. Besides, according to the NIST library,

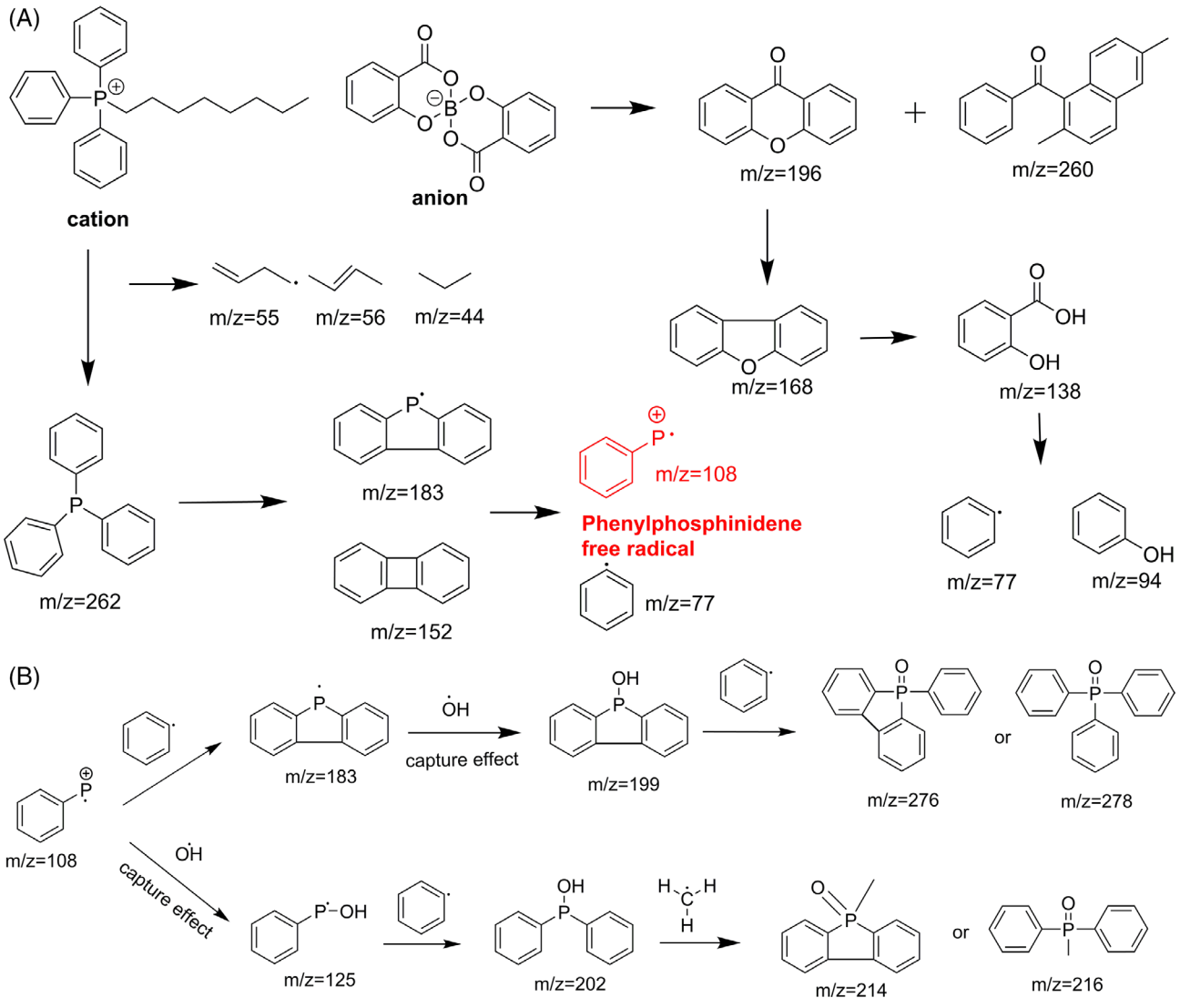

SCHEME 2 Pyrolysis process of (A) [OTP][BScB] and (B) the flame-retarding mode of action in gas phase

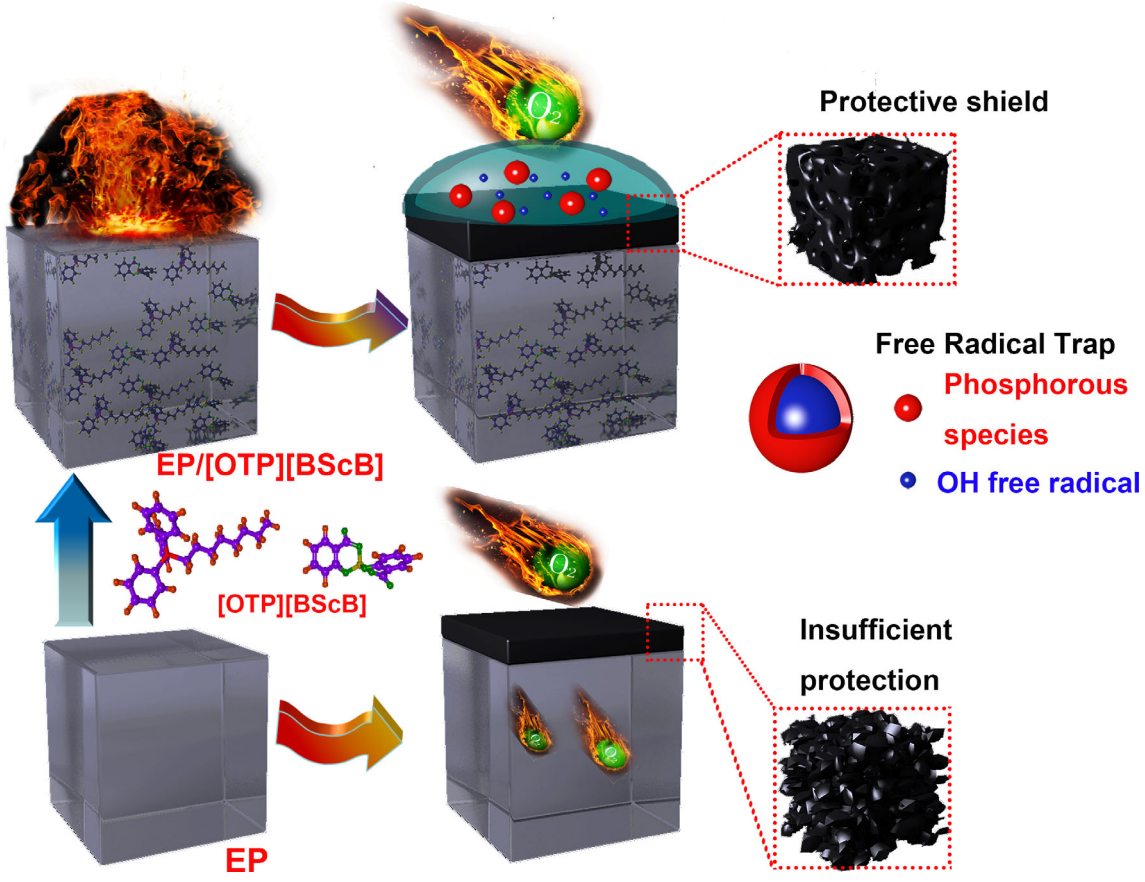

SCHEME 3 Flame-retarding mechanism of [OTP][BScB] in EP

two fragments whose mass-to-charge ratio close to that of the fragment of *m/z* = 277 are shown in Scheme 2B, which represented the possible chemical structure of the fragment of *m/z* = 277.

The flame-retarding mode of action is also illustrated by the above activity of phenylphosphinidene. This free radical captured an OH free radical and combined with the phenyl-based free radical to form phosphorous-containing species, which interrupted the combustion reaction in the gas phase. Therefore, it can be concluded that the absorption peak at 1114/cm in the TG-FTIR of EP/10[OTP][BScB] is due to the P—Ar bond. All in all, the analysis of TG-FTIR and py-GC-MS suggests that [OTP][BScB] plays the flame-retarding role in the gas phase.

3.7 | Flame-retardant mechanism of [OTP][BScB]

From the analysis of residual char and pyrolysis gaseous products, it can be concluded that [OTP][BScB] provided the flame-retarding ability in both phases. In the condensed phase, [OTP][BScB] generated phosphorus- and boron-based acidic compounds to promote char formation. The compact char layer acted as a protective shield to inhibit heat and oxygen permeation and suppress flammable volatile diffusion; in the gas phase, [OTP][BScB] released phosphorus-containing free radicals to capture the hydroxyl free radical, thereby interrupting combustion. Owing to the remarkable flame-retarding action in both phases, EP/[OTP][BScB] exhibited self-extinguishing property during ignition as well as heat and smoke suppression during combustion. The flame-retarding mechanism of [OTP][BScB] is depicted in Scheme 3.

3.8 | Mechanical property of EP and EP composites

To evaluate whether EP/[OTP][BScB] could meet the demand in real conditions, the mechanical property of the composites was estimated. Results of the tensile test of EP composites are given in Table 4. It can be seen clearly that the tensile strength and elongation at break of EP/[OTP][BScB] had a slight fluctuation compared with those of EP. When 3 wt% and 7 wt% [OTP][BScB] were added, EP composites had better mechanical property than EP because of the remarkable reinforcement on each values. Unfortunately, the tensile strength and modulus of EP/10[OTP][BScB] were less than those of EP, but their elongation at break increased. This was probably due to the excessively rigid structure of [OTP][BScB], resulting in a decrease of the cross-linked network of EP, which reduced the modulus obviously. Besides, the overloading of [OTP][BScB] promoted remarkable plasticity for the EP composites, since the T_g of EP/10[OTP][BScB] declined

TABLE 4 Results of tensile test of EP and EP composites

Sample	Tensile strength (Mpa)	Elongation at break (%)	Tensile modulus (Mpa)	Fracture energy (MJ/m^3)
EP	77.0 ± 2.9	12.8 ± 0.8	1358 ± 57	491 ± 22
EP/3[OTP][BScB]	81.8 ± 3.7	13.8 ± 0.8	1451 ± 62	605 ± 42
EP/7[OTP][BScB]	91.1 ± 4.8	12.2 ± 1.3	1628 ± 84	552 ± 76
EP/10[OTP][BScB]	72.5 ± 3.4	16.5 ± 3.2	942 ± 58	641 ± 95

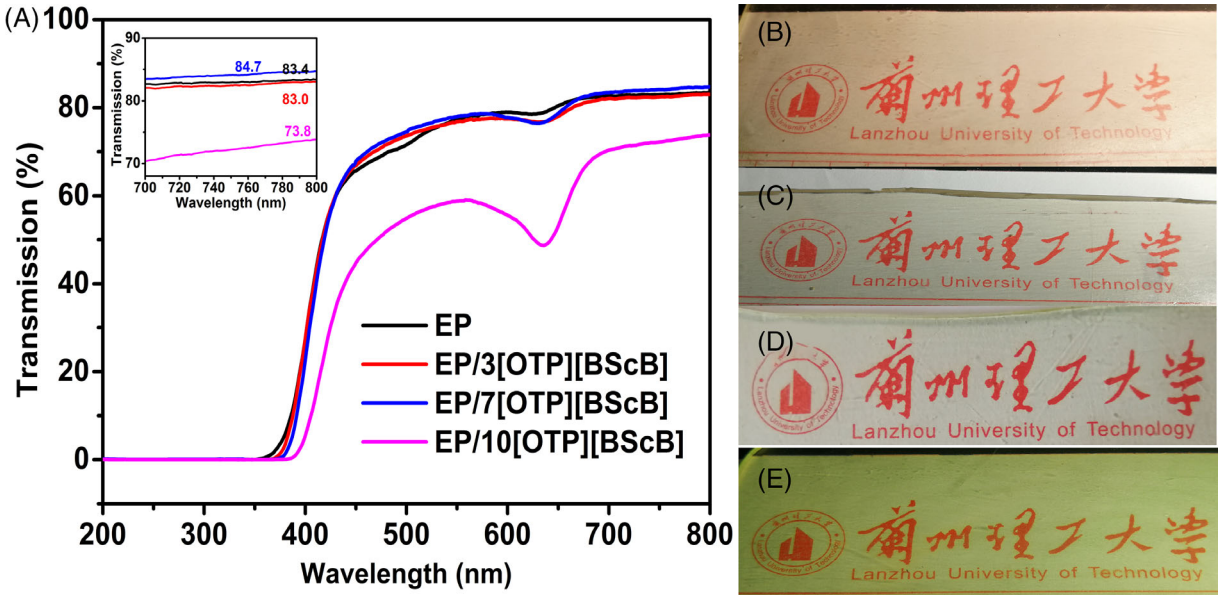

FIGURE 11 (A) UV–vis spectra. digital photographs of (B) EP, (C) EP/3[OTP][BScB], (D) EP/7[OTP][BScB], and (E) EP/10[OTP][BScB]

clearly.[16] However, the interaction between [OTP][BScB] and the EP matrix remained ambiguous, that is, whether the addition of [OTP][BScB] could alleviate its brittle fracture nature or weaken the mechanical property.

To better understand the effect of [OTP][BScB] on the mechanical property of EP, the fracture energy was calculated by the area under the stress–strain curves, whose value represents the toughness of materials.[45] It is noticeable in Table 4 that the values of all EP/[OTP][BScB] samples were significantly higher than those of EP, suggesting that [OTP][BScB] provided EP composite with more energy to resist external force. The possible reason is that the alkyl chain in [OTP][BScB] generated a "tangle effect" in the EP networks. Consequently, external force constantly dissipated and the fracture energy accumulated when crack was extending. Therefore, the plastication behavior was positive to alleviate the brittle fracture of EP with 10 wt% loading. Finally, the tensile result revealed that the mechanical property of EP/[OTP][BScB] is reinforced to some extent.

3.9 | Transparency of EP and EP composites

The influence of [OTP][BScB] on the optical property of EP was investigated by UV–vis spectra and the digital photographs of EP composites in Figure 11. In Figure 11A, the transmission of EP is 83.4% at the wavelength 800 nm. With the incorporation of 3 wt% and 7 wt% [OTP][BScB], the EP composites maintained more than 80% transmission. However, the transmission of the composite decreased with the addition of 10 wt% [OTP][BScB], implying the negative impact of the flame retardant on the optical property when its content is high. From the digital photographs of EP and the composites in Figure 10B–D, the logo and text of Lanzhou University of Technology are clearly seen. Besides, the colorless nature of the EP composites is shown with 3 wt% and 7 wt% IL contents, but EP/10[OTP][BScB] appears slightly green. The transparency and colorlessness of EP/[OTP][BScB] can be the basis for its wide application.

4 | CONCLUSIONS

In this study, IL-chelated orthoborates ([OTP][BScB]) were synthesized successfully and introduced into EP to prepare EP/[OTP][BScB] composites. TGA revealed that the residue yield of EP/[OTP][BScB] increased during thermal degradation. The fire performance indicated that only 3 wt% addition of [OTP][BScB] made EP/3[OTP][BScB] pass the UL-94 V-0 grade and dramatically improved the LOI value to 32.5%. The combustion behavior in the CC test showed that the

values of heat release and smoke production of EP/[OTP][BScB] reduced compared to those of neat EP. The flame-retarding mechanism study indicated that [OTP][BScB] promoted char formation as a protective shield in the condensed phase and released gaseous phosphorus-containing compounds as free radical scavengers in the gas phase. Consequently, [OTP][BScB] showed flame-retarding ability in both phases. Besides, tensile tests suggested that the mechanical property of EP/[OTP][BScB] could be reinforced with 3 wt% and 7 wt % loading. Additionally, the optical property of EP/[OTP][BScB] was maintained to some extent. Considering the above results, [OTP][BScB] could be a promising additive to improve the flame retardancy and mechanical property of EP.

ORCID

Baoping Yang https://orcid.org/0000-0002-4366-6254

REFERENCES

1. Alongi J, Han Z, Bourbigot S. Intumescence: tradition versus novelty. A comprehensive review. *Prog Polym Sci*. 2015;51:28-73.
2. Zhang W, Camino G, Yang R. Polymer/polyhedral oligomeric silsesquioxane (POSS) nanocomposites: an overview of fire retardance. *Prog Polym Sci*. 2017;67:77-125.
3. Velencoso MM, Battig A, Markwart JC, Schartel B, Wurm FR. Molecular firefighting-how modern phosphorus chemistry can help solve the challenge of flame Retardancy. *Angew Chem Int Ed*. 2018;57(33):10450-10467.
4. Vidil T, Tournilhac F, Musso S, Robisson A, Leibler L. Control of reactions and network structures of epoxy thermosets. *Prog Polym Sci*. 2016;62:126-179.
5. Auvergne R, Caillol S, David G, Boutevin B, Pascault P. Biobased thermosetting epoxy: present and future. *Chem Rev*. 2014;114:1082-1115.
6. Wang LR, Yang BP, Guo YL, et al. Synthesis of multielement phosphazene derivative and the study on flame-retardant properties of epoxy resin. *High Perform Polym*. 2020;32(10):1169-1180.
7. Battig A, Markwart JC, Wurm FR, Schartel B. Sulfur's role in the flame retardancy of thio-ether-linked hyperbranched polyphosphoesters in epoxy resins. *Eur Polym J*. 2020;122(5):109390.
8. Kalali EN, Wang X, Wang DY. Multifunctional intercalation in layered double hydroxide: toward multifunctional nanohybrids for epoxy resin. *J Mater Chem A*. 2016;4:2147-2157.
9. Battig A, Markwart JC, Wurm FR, Schartel B. Hyperbranched phosphorus flame retardants: multifunctional additives for epoxy resins. *Polym Chem*. 2019;10(31):4346-4358.
10. Qi Z, Zhang W, He X, Yang R. High-efficiency flame retardency of epoxy resin composites with perfect T_8 caged phosphorus containing polyhedral oligomeric silsesquioxanes (P-POSSs). *Compos Sci Technol*. 2016;127:8-19.
11. Li Z, Zhang JH, Dufosse F, Wang DY. Ultrafine nickel nanocatalyst-engineering of an organic layered double hydroxide towards a super-efficient fire-safe epoxy resin via interfacial catalysis. *J Mater Chem A*. 2018;6:8488-8498.
12. Qu ZC, Wu K, Jiao EX, et al. Surface functionalization of few-layer black phosphorene and its flame retardancy in epoxy resin. *Chem Eng J*. 2020;382:122991.
13. Zhang ZD, Qin JY, Zhang WC, Pan YT, Wang DY, Yang RJ. Synthesis of a novel dual layered double hydroxide hybrid nanomaterial and its application in epoxy nanocomposites. *Chem Eng J*. 2020;381:122777.
14. Shao ZB, Zhang MX, Li Y, Han Y, Ren L, Deng C. A novel multifunctional polymeric curing agent: synthesis, characterization, and its epoxy resin with simultaneous excellent flame retardance and transparency. *Chem Eng J*. 2018;345:471-482.
15. Huddleston JG, Willauer HD, Swatloski RP, Visser AE, Rogers RD. Room temperature ionic liquids as novel media for 'clean' liquid-liquid extraction. *Chem Commun*. 1998;16:1765-1766.
16. Scott MP, Brazel CS, Benton MG, Mays JW, Holbrey JD, Rogers RD. Application of ionic liquids as plasticizers for poly(methyl methacrylate). *Chem Commun*. 2002;13:1370-1371.
17. Li X, Feng Y, Chen C, et al. Highly thermally conductive flame retardant epoxy nanocomposites with multifunctional ionic liquid flame retardant-functionalized boron nitride nanosheets. *J Mater Chem A*. 2018;6:20500-20512.
18. Hisashi K, Masayoshi W. Anionic polymerization of methyl methacrylate in an ionic liquid. *Polym Adv Technol*. 2008;19:1441-1444.
19. Tang Z, Li Y, Zhang YJ, Jiang P. Oligomeric siloxane containing triphenylphosphonium phosphate as a novel flame retardant for polycarbonate. *Polym Degrad Stab*. 2012;97:638-644.
20. Li CX, Ma C, Li J. Highly efficient flame retardant poly(lactic acid) using imidazole phosphate poly(ionic liquid). *Polym Adv Technol*. 2020;31(8):1765-1775.
21. Xiao F, Wu K, Luo F, et al. Influence of ionic liquid-based metal–organic hybrid on thermal degradation, flame Retardancy, and smoke suppression properties of epoxy resin composites. *J Mater Sci*. 2018;53:10135-10146.
22. Xiao F, Wu K, Luo F, et al. An efficient phosphonate-based ionic liquid on flame retardancy and mechanical property of epoxy resin. *J Mater Sci*. 2017;52(24):13992-14003.
23. Shi YQ, Fu T, Xu YJ, Li DF, Wang XL, Wang YZ. Novel phosphorus-containing halogen-free ionic liquid toward fire safety epoxy resin with well-balanced comprehensive performance. *Chem Eng J*. 2018;354:208-219.
24. Maka H, Spychaj T, Pilawka R. Epoxy resin/ionic liquid systems: the influence of Imidazolium Cation size and anion type on reactivity and Thermomechanical properties. *Ind Eng Chem Res*. 2012;51:5197-5206.
25. Xu YJ, Wang J, Tan Y, Qi M, Chen L, Wang YZ. A novel and feasible approach for one-pack flame-retardant epoxy resin with long pot life and fast curing. *Chem Eng J*. 2018;337:30-39.
26. Nguyen L, Livi S, Soares BG, Pruvost S, Duchet RJ, Gerard JF. Ionic liquids: a new route for the design of epoxy networks. *ACS Sustain Chem Eng*. 2016;4:481-490.
27. Livi S, Silva AA, Thimont Y, et al. Nanostructured thermosets from ionic liquid building block–epoxy prepolymer mixtures. *RSC Adv*. 2014;4:28099-28106.
28. Nguyen L, Livi S, Pruvost S, Soares BG, Duchet RJ. Ionic liquids as reactive additives for the preparation and modification of epoxy networks. *J Polym Sci Polym Chem*. 2014;52:3463-3471.
29. Sonnier R, Dumazert L, Livi S, et al. Flame retardancy of phosphorus-containing ionic liquid based epoxy networks. *Polym Degrad Stab*. 2016;134:186-193.
30. Guo YL, Cui JF, Guo JH, Zhang HJ, Wang LR, Yang BP. Modification of POSS hybrids by ionic liquid simultaneously prolonging time to ignition and improving flame retardancy for polystyrene. *J Polym Res*. 2020;27(4):101.
31. Intharapat P, Nakason C, Kongnoo A. Preparation of boric acid supported natural rubber as a reactive flame retardant and its properties. *Polym Degrad Stab*. 2016;128:217-227.
32. Xu W, Wang LM, Nieman RA, Angell CA. Ionic liquids of chelated Orthoborates as model ionic Glassformers. *J Phys Chem B*. 2003;107:11749-11756.
33. Markwart JC, Battig A, Velencoso MM, Pollok D, Schartel B, Wurm FR. Aromatic vs. aliphatic Hyperbranched Polyphosphoesters as flame retardants in epoxy resins. *Molecules*. 2019;24(21):3901.
34. Yang BP, Wang LR, Guo YL, et al. Synthesis of a novel phosphate-containing highly transparent PMMA copolymer with enhanced thermal and flame retardant properties. *Polym Adv Technol*. 2019;31(3):472-481.

35. Geoffroy L, Davesne Al, Bellayer S, et al. 3D printed sandwich materials filled with hydrogels for extremely low heat release rate. *Polym Degrad Stab*. 2020;179:109269.
36. Zhang L, Wang Q, Jian RK, Wang DY. Bioinspired iron-loaded polydopamine nanospheres as green flame retardants for epoxy resin via free radical scavenging and catalytic charring. *J Mater Chem A*. 2020;8(5):2529-2538.
37. Schartel B, Hull TR. Development of fire-retarded materials—interpretation of cone calorimeter data. *Fire Mater*. 2007;31:327-354.
38. Lu HD, Wilkie CA. Synergistic effect of carbon nanotubes and decabromodiphenyl oxide/Sb_2O_3 in improving the flame retardancy of polystyrene. *Polym Degrad Stab*. 2019;95:564-571.
39. Yan YW, Chen L, Jian RK, Kong S, Wang YZ. Intumescence: an effect way to flame retardance and smoke suppression for polystryene. *Polym Degrad Stab*. 2012;97:1423-1431.
40. Bourbigot S, Bras ML, Gengembre L, Delobel R. XPS study of an intumescent coating application to the ammonium polyphosphate/pentaerythritol fire-retardant system. *Appl Surf Sci*. 1994;81:299-307.
41. Naik AD, Bourbigot S, Bellayer S, et al. Salen complexes as fire protective agents for thermoplastic polyurethane: deep electron paramagnetic resonance spectroscopy investigation. *ACS Appl Mater Inter*. 2018;10:24860-24875.
42. Sut A, Greiser S, Jäger C, Schartel B. Aluminium diethylphosphinate versus ammonium polyphosphate: a comprehensive comparison of the chemical interactions during pyrolysis in flame-retarded polyolefine/poly(phenylene oxide). *Thermochim Acta*. 2016;640:74-84.
43. Xu MJ, Xu GR, Leng Y, Li B. Synthesis of a novel flame retardant based on cyclotriphosphazene and DOPO groups and its application in epoxy resins. *Polym Degrad Stab*. 2016;123:105-114.
44. Keck H, Kuchen W, Tommes P. The Phenylphosphinidene C6H5P is stable under Unimolecular conditions - a theoretical prediction. *Phosphorus Sulfur Silicon Relat Elem*. 1996;111(1–4):40-40.
45. Li Z, Wang DY. Nano-architectured mesoporous silica decorated with ultrafine Co_3O_4 toward an efficient way to delaying ignition and improving fire retardancy of polystyrene. *Mater Design*. 2017;129:69-81.

SUPPORTING INFORMATION

Additional supporting information may be found online in the Supporting Information section at the end of this article.

How to cite this article: Guo Y, Chen X, Cui J, Guo J, Zhang H, Yang B. Effect of ionic liquid octyltriphenylphosphonium-chelated orthoborates on flame retardance of epoxy. *Polym Adv Technol*. 2021;32:1579–1596. https://doi.org/10.1002/pat.5195